Journal of Alloys and Compounds 844 (2020) 156096

Contents lists available at ScienceDirect

Journal of Alloys and Compounds

journal homepage: http://www.elsevier.com/locate/jalcom

# Chemical stabilization of $Eu^{2+}$ in $LuPO_4$ and $YPO_4$ hosts and its peculiar sharp line luminescence

Justyna Zeler [a, b], Megi Sulollari [b, 1], Andries Meijerink [c], Marco Bettinelli [d], Eugeniusz Zych [b, *]

[a] Department of Physics CICECO-Aveiro Institute of Materials University of Aveiro Campus de Santiago, Aveiro, Portugal
[b] Faculty of Chemistry, University of Wroclaw, 14 F. Joliot-Curie Street, 50-383, Wroclaw, Poland
[c] Condensed Matter and Interfaces, Debye Institute for Nanomaterials Science, Utrecht University, Princetonplein 1, 3584 CC, Utrecht, the Netherlands
[d] Luminescent Materials Laboratory, Department of Biotechnology, University of Verona and INSTM, UdR Verona, Strada Le Grazie 15, 37134, Verona, Italy

ARTICLE INFO

*Article history:*
Received 25 March 2020
Received in revised form
26 May 2020
Accepted 15 June 2020
Available online 20 June 2020

*Keywords:*
$Eu^{2+}$ luminescence
Vibronic progression
Lu/$YPO_4$ crystals

ABSTRACT

The efficient $4f^65d \rightarrow 4f^7$ (d-f) luminescence from $Eu^{2+}$ is well-known for host lattices where $Eu^{2+}$ is substituted on a divalent (e.g. $Ca^{2+}$, $Sr^{2+}$) or monovalent (e.g. $Na^+$, $K^+$) cation site. Only recently some studies appeared concerning d-f emission from $Eu^{2+}$ on a trivalent cation site. The stable $Eu^{2+}$ emission was observed in X-ray irradiated $LuPO_4$:$Eu^{3+}$ crystals where $Eu^{2+}$ is produced through trapping of conduction band electrons generated by X-ray absorption. Here, we demonstrated that $Eu^{2+}$ can also be *chemically* stabilized in $YPO_4$ and $LuPO_4$ through co-doping with a tetravalent charge compensator: $Hf^{4+}$. In orthophosphate crystals doubly doped with Eu and Hf, the characteristic $Eu^{2+}$ emission is observed at low temperatures without the need for X-ray irradiation. The excitation and emission spectra show strong and narrow zero-phonon lines and a rich vibronic structure. In the excitation spectra a multitude of zero-phonon transitions to individual crystal field components of $^7F_J$ multiplets in the $4f^6(^7F_J)5d$ excited state was observed for $Eu^{2+}$ in both $LuPO_4$ and $YPO_4$. Analysis of the spectra is consistent with a slightly larger crystal field splitting for $Eu^{2+}$ on the smaller $Lu^{3+}$ site (compared to $Y^{3+}$). The observation of many $4f^6(^7F_J)5d$ electronic origins make these systems to be model compounds for testing the validity of theoretical models for energy level calculations of $4f^65d$ states of $Eu^{2+}$.



## 1. Introduction

$Eu^{2+}$ emission in different inorganic hosts has attracted enormous attention driven by its attractive application-properties [1–4]. The characteristics of $Eu^{2+}$ luminescence are strongly dependent on the nature of ligands, $Eu^{2+}$-ligand distances and the ion local symmetry [5–13]. Consequently, a wide range of emission colors (from UV to infrared) may be obtained introducing $Eu^{2+}$ into different hosts. Even within orthophosphate matrices the $Eu^{2+}$ emission wavelength can vary quite significantly. For example, in $NaMgPO_4$ and $KSrPO_4$, $Eu^{2+}$ ions show blue emission [14–17] while it is green in $NaCaPO_4$ and $KCaPO_4$ [18,19].

For years it was generally accepted that $Eu^{2+}$ cannot generate luminescence when substituted for 3+ metal site [20] while its emission was usually easily observed when it substituted into 2+ or 1+ cation site. In fact, in many cases, such an aliovalent substitution is also hampered by the ionic radii difference as $Eu^{2+}$ (1.25 Å for coordination number CN = 8 [21]) is typically significantly larger than triply ionized ions constituting the host materials. It is only recently that some reports appeared on $Eu^{2+}$ luminescence in $Y_3Al_5O_{12}$ (YAG) host [22–24]. In some of those cases, stabilization of $Eu^{2+}$ could be improved when the doping was executed using $EuF_2$ or EuS in the reacting mixture of oxides.

Here, we report on $Eu^{2+}$ luminescence in orthophosphates $YPO_4$ and $LuPO_4$ where $Eu^{2+}$ is situated on a $Y^{3+}$ or $Lu^{3+}$ site. According to recent studies of Dorenbos [25,26], the $^8S_{7/2}$ ground state of $Eu^{2+}$ is located at ~3.5–3.6 eV below the bottom of conduction band of $LuPO_4$ or $YPO_4$. The lowest $4f^65d^1$ excited state of this ion is then about 0.5 eV and 0.4 eV below the bottom of $YPO_4$ and $LuPO_4$ conduction band, respectively. In principle, this is sufficient for the appearance of $Eu^{2+}$ luminescence at lower temperatures. Indeed,

* Corresponding author.
*E-mail address:* eugeniusz.zych@chem.uni.wroc.pl (E. Zych).
[1] Present address: Department of Biomedical Engineering, University of West Attica, 122 10 Athens, Greece.

https://doi.org/10.1016/j.jallcom.2020.156096
0925-8388/

we recently showed that, in the $LuPO_4:Eu^{3+}$ storage phosphor, a fraction of the dopant can be converted to $Eu^{2+}$ upon the impact of X-rays and these ions remain stable for long time at room temperature (RT) and show the characteristic $4f^65d \rightarrow 4f^7$ emission from $Eu^{2+}$ between 20 K and RT [27]. In the excitation spectra of the $LuPO_4:Eu^{2+}$, at liquid helium temperature, an exceptionally rich fine structure with a large number of narrow lines were observed and analyzed in depth [27].

Very recently, Laguta at al. have published results of EPR studies on sintered ceramics and single crystals of $YPO_4$ and $LuPO_4$ singly (Eu) or doubly (Eu,Hf) activated [28]. That work was mostly driven by the quest for the excited carriers trapping sites in these materials when exposed to X-rays. In the end of the present paper, we shall shortly refer to these results, as the comparison of EPR and PL data of basically the same materials allows also to obtain interesting insight.

These observations posed the question about the possibility of synthesizing $LuPO_4$ and its structural analogue $YPO_4$ activated with $Eu^{2+}$ by means of a *chemical* approach rather than exposure to ionizing radiation. In the present study, we demonstrate that chemically stable $Eu^{2+}$ ions can be *directly* incorporated into $YPO_4$ and $LuPO_4$ single crystals through charge compensation with $Hf^{4+}$, resulting in the characteristic $Eu^{2+}$ photoluminescence at RT and below.

## 2. Materials and methods

### 2.1. Crystals growth

$LuPO_4$:Eu,Hf and $YPO_4$:Eu,Hf single crystals were grown by a $Pb_2P_2O_7$-flux method under the ambient pressure and atmosphere according to procedure reported in literature [29–33]. The starting materials were: lutetium oxide, $Lu_2O_3$ (99.9%, Alfa Aesar) or yttrium oxide, $Y_2O_3$ (99.99%, Alfa Aesar), europium oxide, $Eu_2O_3$ (99.99%, Strem Chemicals), and hafnium oxide, $HfO_2$ (98%, Aldrich) – all supplied by the Stanford Materials, USA. These reagents were combined in stoichiometric ratios to produce $(Lu_{0.999}\ Eu_{0.0005}Hf_{0.0005})PO_4$ and $(Y_{0.999}\ Eu_{0.0005}Hf_{0.0005})PO_4$. The source of phosphate groups was the flux itself. It consisted of lead oxide (PbO, >99.9%, Aldrich) and diammonium hydrogen phosphate, ($(NH_4)_2HPO_4$, >99.0, Fluka), which, at higher temperatures, react to give the actual $Pb_2P_2O_7$ flux. To create the flux, 25.00 g of PbO and 14.79 g of $(NH_4)_2HPO_4$ were used. A mixture of all chemicals was placed in a Pt crucible, transferred into a cold muffle furnace and heated to 1300 °C. The crystals growth took place in the course of the slow cooling of furnace from 1300 °C to 950 °C. The crystals were recovered by dissolving the flux in warm dilute $HNO_3$. Each batch produced a number of crystals of various sizes (~1–3x2-5x0.5 mm) and the largest of them were chosen for the spectroscopic experiments (see Fig. S1).

### 2.2. Methods

The single crystalline form of the investigated crystals was verified using KUMA KM4 diffractometer. It used graphite-monochromated Mo-Kα radiation and the measurements were performed at room temperature. The chemical composition of the investigated crystals was verified using an EDAX energy-dispersive X-ray spectroscopy (EDX) attachment of a Hitachi S–3400 N scanning electron microscope. For comparison, also a singly-doped $LuPO_4$:Eu crystal was analyzed. The measurements of photoluminescence (PL) and excitation (PLE) spectra and luminescence decay curves in the range of 20–300 K were performed using an FLS980–sm Fluorescence Spectrometer from Edinburgh Instruments Ltd. The samples were mounted on a Lake Shore Cryotronics closed-cycle helium cryostat holder using a Silver Adhesive 503 supplied by Electron Microscopy Sciences. A 450 W continuous Xe arc lamp was used as the excitation source to measure PL and PLE spectra and an EPLED-360 nm ps pulsed (~950 ps pulse width) light emitting diode - for recording luminescence decays. The TMS302-X single grating excitation and emission monochromators of 30 cm focal lengths were utilized in the excitation and emission channels. In PL and PLE spectra, the emitted light was recorded by means of a Hamamatsu R928P high-gain photomultiplier and the luminescence decay traces were taken with a F-G05 photomultiplier featuring a Hamamatsu H5773-04 detector. The emission spectra were corrected for the spectral response of the emission detection system and excitation spectra were corrected for the variation in incident light intensity. The IR spectra of $LuPO_4$:Eu powders (crystals ground in an agate mortar) suspended in nujol were recorded with an IFS 66/s Bruker spectrometer in the range of 50–4000 $cm^{-1}$ at RT.

## 3. Results and discussion

Figure S1 presents a photograph of the investigated crystals. The crystallographic analysis confirmed their monocrystallinity and tetragonal structure, space group $I4_1/amd$. For $LuPO_4$:Eu,Hf the following unit cell parameters were found: a = 6.690(19), b = 6.71(2), c = 5.86(7) Å, V = 263.3 $Å^3$ and for $YPO_4$:Eu,Hf these were a = 6.823(6), b = 6.823(6), c = 6.064(18) Å, V = 282.3(8) $Å^3$. These results are in very good agreement with the literature data [34].

The EDX analysis (see Fig. S2) proved that the concentration of Eu and Hf in the $YPO_4$:Eu,Hf crystal was close to the nominal 0.05 mol%. Repeating measurements produced results ranging the 0.05–0.06 mol%. The EDX results for $LuPO_4$:Eu,Hf presented Hf content much higher than Eu concentration (0.4–0.6 mol% vs. 0.008–0.011 mol%). This difference in the content of Eu and Hf in the two crystals becomes understandable upon the comparison of ionic radii of the metal ions. $Hf^{4+}$, whose radius is 0.83 Å (CN = 8), is by 15% smaller than $Lu^{3+}$ (0.977 Å) but by 18.5% smaller than $Y^{3+}$ (1.019 Å). Thus, incorporation of Hf is supposed to be easier into $LuPO_4$ than to $YPO_4$, exactly as found by EDX analysis. The situation is different when substitution of Lu and Y by Eu is considered. $Eu^{3+}$ (1.066 Å) is larger than $Lu^{3+}$ by 9% and only by 4.6% larger than $Y^{3+}$. $Eu^{2+}$ (1.25 Å) is much larger than $Lu^{3+}$ (28%) and compared to $Y^{3+}$ the difference is 22.7%, still very significant but definitely less profound. Hence, incorporation of Eu, whether $Eu^{3+}$ or $Eu^{2+}$ is supposed to be less efficient in $LuPO_4$ than in $YPO_4$. And it is exactly what the measurements show. The singly-doped $LuPO_4$:0.05mol% Eu crystal showed ~0.06 mol% of Eu concentration and no Hf was detected. This concentration is close to the nominal content and much higher than in $LuPO_4$:Eu,Hf. This is reasonable bearing in mind that in the presence of Hf mainly $Eu^{2+}$ enters the host while incorporation of $Eu^{3+}$ is hindered. Hence, the EDX analysis confirmed that Hf was indeed incorporated into both crystals. Recently, we reported the observation of $Eu^{2+}$ emission in $LuPO_4:Eu^{3+}$. The reduction of $Eu^{3+}$ was accomplished in an X-ray irradiated, polycrystalline pellet of $LuPO_4$:Eu [27]. Since the stability of $Eu^{2+}$ in the $LuPO_4$ ceramic host has been proved, together with its ability to generate blue emission due to the $5d^14f^6 \rightarrow 4f^7$ transition, it is interesting to investigate if $Eu^{2+}$ can be chemically stabilized in the $LuPO_4$ or $YPO_4$ lattices by means of co-doping with $Hf^{4+}$. It was anticipated that, in the presence of $Hf^{4+}$, a charge-neutral substitution process expressed by Eqs. (1) and (2) might be accomplished as follows:

$$2Lu^{X}_{Lu} = Eu'_{Lu} + Hf^{\bullet}_{Lu} \quad (1)$$

$$2Y^{X}_{Y} = Eu'_{Y} + Hf^{\bullet}_{Y} \quad (2)$$

Here and throughout this paper, we use the Kröger–Vink notation of defects recommended by IUPAC [35]. In Fig. 1, the emission spectra of $LuPO_4$:Eu,Hf (Fig. 1a) and $YPO_4$:Eu,Hf (Fig. 1b) recorded upon 350 nm excitation in the temperatures range of 20–300 K are presented. At 250–300 K, both crystals show a very similar emission bands peaking around ~430 nm with FWHM of ~19–21 nm (~1000 $cm^{-1}$). This luminescence is assigned to the $4f^65d^1 \rightarrow {}^8S_{7/2}$ transition of $Eu^{2+}$. The energy of the luminescence agrees with predictions of Dorenbos model and is in line with the data reported for the $Eu^{2+}$ emission in the X-ray irradiated $LuPO_4$ [36]. Note that the samples contain also some $Eu^{3+}$ which upon properly chosen excitation produces its characteristic orange-red luminescence, see Fig. S3. The simultaneous presence of emitting $Eu^{2+}$ and $Eu^{3+}$ ions in phosphors was reported previously for a few hosts [37–39]. Yet, in the cited papers the lattices offered both 2+ and 3+ metals sites, and this is an important difference compared to our orthophosphates.

As the temperature decreases, a characteristic fine structure appears. At 20 K, a well-resolved vibronic structure of the $Eu^{2+}$ emission is observed with a sharp zero-phonon line (ZPL) at 425.80 nm ($LuPO_4$) or 424.40 nm ($YPO_4$). As it is clear in Fig. 1, the intensities of the vibronic lines relative to the ZPL are higher in $LuPO_4$ than in $YPO_4$. Consequently, it is inferred that in $LuPO_4$:$Eu^{2+}$,$Hf^{4+}$ (Fig. 1a) the electron-phonon coupling is larger than in $YPO_4$:$Eu^{2+}$,$Hf^{4+}$ (Fig. 1b) [40–43]. To obtain evidence for the role of charge compensation by $Hf^{4+}$ to stabilize $Eu^{2+}$, also the measurements were performed on a singly doped $LuPO_4$:Eu single crystal. Under the identical measuring conditions, no sign of $Eu^{2+}$ emission was found (see Fig. S4 of the supporting information), clearly showing that charge compensation by $Hf^{4+}$ is responsible for the presence of $Eu^{2+}$ in $LuPO_4$:Eu crystals and that chemical stabilization by co-doping with $Hf^{4+}$ is an alternative to X-ray irradiation to realize $Eu^{2+}$-doped $LuPO_4$.

An analysis of the electron-phonon coupling and assignment of the vibronic lines similar to that presented in Ref. [27] for the X-ray irradiated $LuPO_4$:Eu is performed. Combining the emission spectra (in energy scale) at 20 K with the relative IR spectra (300 K) allow the various vibronic lines assignment to coupling with specific host phonons labelled in order of increasing energy from $\nu_1$ to $\nu_9$. These data are presented in Fig. 2a ($LuPO_4$:Eu,Hf), and Fig. 2b ($YPO_4$:Eu,Hf). For both hosts, a vibronic progression due to coupling with the same vibrational modes is observed. The analysis is difficult as coupling with different modes is found in these compositions. The strongest coupling is observed with the Ln-O modes ($\nu_1$-$\nu_7$ = 50–700 $cm^1$), while coupling to the orthophosphate-related phonons ($\nu_{9a}$-$\nu_{9c}$ = 800-1200 $cm^{-1}$) was significantly lower [44]. Weaker coupling with vibrational modes localized on the phosphate groups can be expected as the distance to the $Eu^{2+}$ ion is larger. The results are summarized in Table 1. These data agree with the previous results for $Eu^{2+}$ emission in the X-ray irradiated $LuPO_4$:Eu polycrystalline ceramic material [27]. A comparison of the results for the two materials shows the presence of a blue shift of the ZPL line in $YPO_4$:$Eu^{2+}$,$Hf^{4+}$ of about 1.4 nm (78 $cm^{-1}$) in reference to the ZPL in $LuPO_4$:$Eu^{2+}$,$Hf^{4+}$. This is explained by the presence of a stronger crystal field in the latter as $Lu^{3+}$ is smaller than $Y^{3+}$ (ionic radii 0.977 Å for $Lu^{3+}$ and 1.019 Å for $Y^{3+}$, for CN = 8) [21]. The shorter $Eu^{2+}$-$O^{2-}$ distances for $Eu^{2+}$ on the site of smaller $Lu^{3+}$ ion will result in a larger crystal field splitting which shifts the lowest energy $4f^65d^1$ state to lower energies.

The excitation spectra of $Eu^{2+}$ luminescence at 150 and 20 K in $LuPO_4$ and $YPO_4$ crystals are presented in Fig. 3a and b, respectively. At the higher temperature two broad bands in the 240–320 nm and 330–430 nm spectral regions were observed in both compositions. These excitation bands are induced by $4f^7 \rightarrow 4f^65d^1$ transitions of $Eu^{2+}$, as previously shown [27]. The lower-energy band in both orthophosphates show a very rich fine structure at 20 K. In line with our analysis in Ref. [27], these intense narrow excitation lines at 20 K are related to the transitions from the ${}^8S_{7/2}$ ground level of $Eu^{2+}$ to the $Eu^{3+}$-like ${}^7F_{0\text{-}6}$ core levels of the $4f^6({}^7F_{0\text{-}6})5d^1$ excited configuration of $Eu^{2+}$ ions. At this point, we may note that the spectroscopic characteristics of the $Eu^{2+}$ chemically stabilized in the two orthophosphates by $Hf^{4+}$ are very similar to those reported for $Eu^{2+}$ states generated in $LuPO_4$:Eu upon the X-rays impact [27].

In Fig. 4, the 20 K photoluminescence of $Eu^{3+}$ in $YPO_4$ (blue line) is shown to compare energies of the $4f^6({}^7F_J)$ levels of $Eu^{3+}$ with those observed in the $4f^6({}^7F_J)5d$ excitation spectrum of $Eu^{2+}$ in the (Eu,Hf) co-doped crystal (black line). Due to selection rules [45] and low instrumental response beyond 800 nm, the luminescence of $Eu^{3+}$ could be recorded only for the ${}^5D_0 \rightarrow {}^7F_{1\text{-}4}$ transitions. The overall correlation of both spectra is evident, which supports the assignment of the $Eu^{2+}$ excitation lines to the transitions to the ${}^7F_J$ core levels of the $4f^6({}^7F_{0\text{-}6})5d^1$ excited configuration. Nevertheless, the splitting of the components of different ${}^7F_J$ levels in the case of the ${}^8S_{7/2} \rightarrow 4f^6({}^7F_J)5d^1$ excitation (black letters in Fig. 4) is larger than that for the ${}^7F_J$ levels observed in the luminescence of $Eu^{3+}$ in the host (blue line). This difference may be taken as a direct measure of the effect of interaction/coupling of the $4f^6$ and $5d^1$ configurations in the $4f^6({}^7F_J)5d^1$ excited state of $Eu^{2+}$ [27].

A similar deviation between the $4f^n$ splitting and the splitting for the same $4f^n$ configuration in a$4f^n5d^1$ excited state was previously observed in the $4f^n \rightarrow 4f^{n-1}5d^1$ excitation spectra of trivalent lanthanides, also in $LuPO_4$ and $YPO_4$ [46]. The observation of many well-resolved zero-phonon lines for $4f^7 \rightarrow 4f^6({}^7F_J)5d^1$ transitions on $Eu^{2+}$ in $LuPO_4$ and $YPO_4$ allows the construction of an accurate energy level diagram for $Eu^{2+}$ in both host lattices Based on these

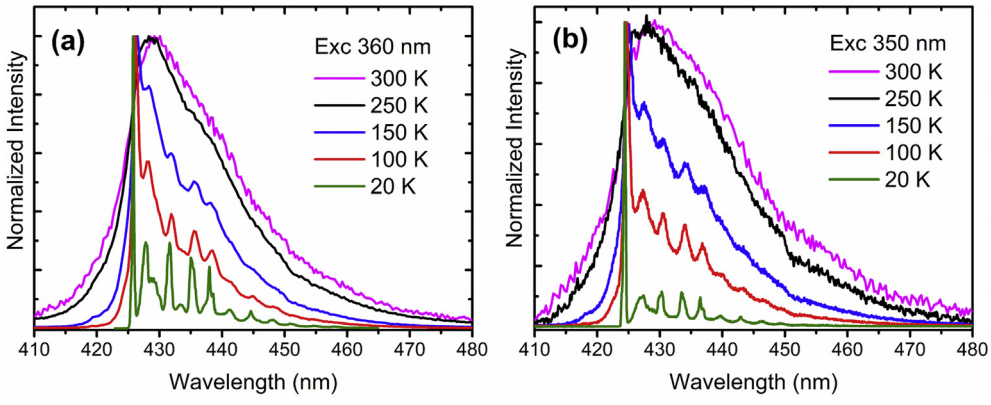


**Fig. 1.** The emission spectra obtained upon the 350 nm excitation of $LuPO_4$:Eu,Hf (a) and $YPO_4$:Eu,Hf (b) in 20–250 K temperature range.

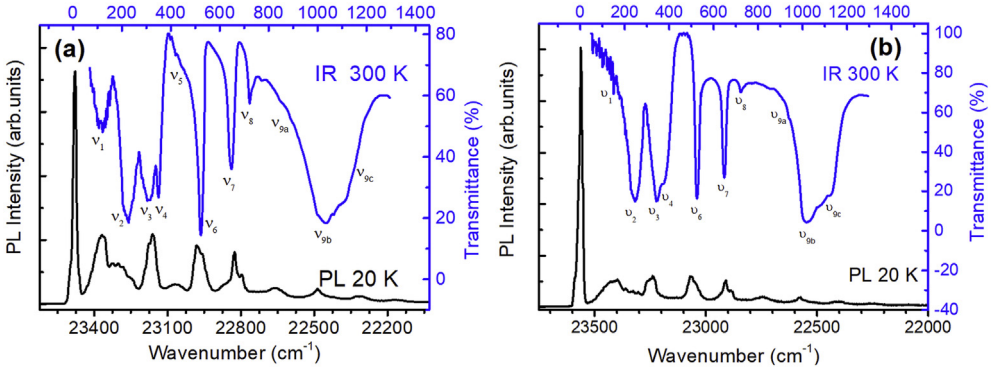


**Fig. 2.** The low temperature (20 K) PL spectra upon 350 nm excitation of $LuPO_4$:Eu,Hf (a) and $YPO_4$:Eu,Hf (b) combined with RT IR spectra for the analysis of the vibronic lines.

**Table 1**
Positions of the ZPL and vibronic lines observed in the emission spectrum of $Eu^{2+}$ in $LuPO_4$:Eu,Hf and $YPO_4$:Eu,Hf at 20 K. The vibronic lines are labelled 1, 2, 3, 4, 5, 6, 7, 9 according to increasing energy of vibration ν.

| Emission | | | | | | |
|---|---|---|---|---|---|---|
| $LuPO_4$ | | | | $YPO_4$ | | |
| Transition | λ (nm) | E ($cm^{-1}$) | Energy difference (with respect to ZPL) ($cm^{-1}$) | λ (nm) | E ($cm^{-1}$) | Energy difference (with respect to ZPL) ($cm^{-1}$) |
| **$4f^6(^7F_0)5d^1 \rightarrow {}^8S_{7/2}$** | **425.80** | **23486.55** | **0** | **424.40** | **23562.70** | **0** |
| $\nu_1$ | 427.90 | 23370.90 | 115.60 | 427.10 | 23414.85 | 147.85 |
| $\nu_2$ | 429.70 | 23272.80 | 213.70 | 428.80 | 23321.35 | 241.35 |
| $\nu_3$ | 431.55 | 23171.90 | 314.65 | 430.35 | 23236.55 | 326.15 |
| $\nu_5$ | 433.60 | 23061.70 | 424.85 | – | – | – |
| $\nu_6$ | 435.30 | 22971.50 | 515.05 | 434.00 | 23041.85 | 520.85 |
| $\nu_7$ | 437.80 | 22840.30 | 646.25 | 436.40 | 22916.00 | 646.70 |
| $\nu_{9a}$ | 441.35 | 22656.75 | 829.80 | 439.60 | 22747.70 | 815.00 |
| $\nu_{9b}$ | 444.80 | 22480.75 | 1005.80 | 443.10 | 22567.15 | 995.55 |
| $\nu_{9c}$ | 447.90 | 22325.10 | 1161.45 | 446.15 | 22414.10 | 1148.60 |

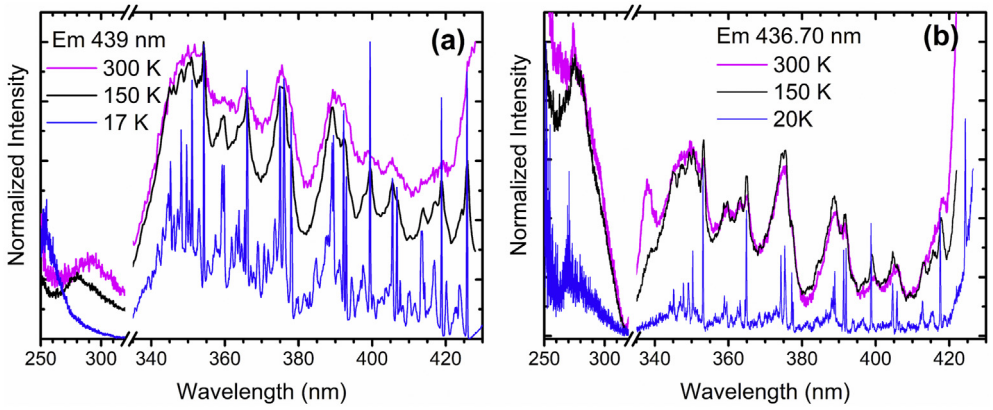


**Fig. 3.** The excitation spectra of $Eu^{2+}$ ions in $LuPO_4$:Eu,Hf (a) and $YPO_4$:Eu,Hf (b) at 20, 150 and 300 K for wavelengths indicated in the panels.

accurate observations, $YPO_4$:$Eu^{2+}$ and $LuPO_4$:$Eu^{2+}$ can serve as a model system for comparison with and testing of the validity of (new) theoretical models. These experimental data would be of particular significance to verify the results of calculation of the $4f^65d^1$ energy levels taking into account e.g. crystal field splitting, relativistic effects, and spin-orbit coupling in addition to Coulomb interactions [46–50]. For the commonly observed broad band 4f↔5d absorption and emission spectra without fine structure, it is easy to obtain a reasonable agreement and, at the same time, it is, therefore, difficult to determine how accurate or correct the model is. The observation of so many well-resolved electronic origins (ZPLs), however, provides a rigorous test for theoretical models. Only if the theoretical calculations reproduce the positions of all these lines with high accuracy, it is evident that the model correctly takes into account the various interactions and effects that give rise to the complex energy level structure of the $4f^65d^1$ configuration.

In the Supplementary Material, a detailed analysis of the electronic ZPL lines and related vibronic components is presented separately for each $^7F_J$ (J = 0, 1, 2, 3, 4, 5 or 6) group of the excitation transitions in both hosts. In Figs. S5–S11, the spectra are presented for $YPO_4$:Eu,Hf. Analogous figures for $LuPO_4$:Eu,Hf are not presented as they appeared indistinguishable from those presented in Refs. [27] for the X-ray irradiated $LuPO_4$:Eu. For both compositions, $LuPO_4$:Eu,Hf and $YPO_4$:Eu,Hf, the results of the analysis are

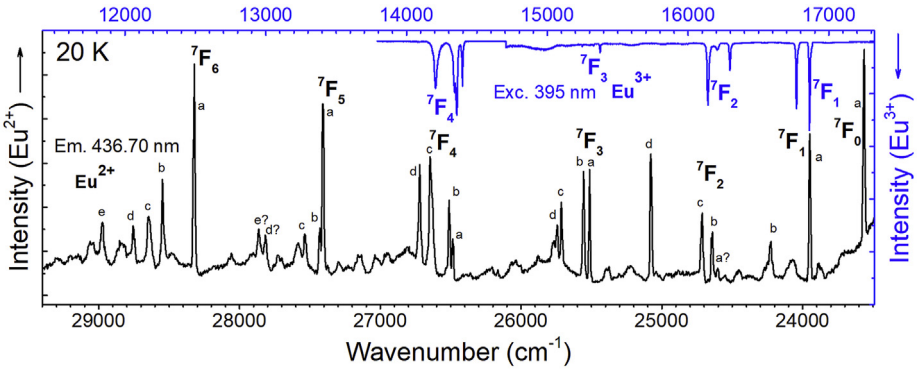


**Fig. 4.** The low temperature (20 K) PLE spectrum of $Eu^{2+}$ emission of $YPO_4$:Eu,Hf crystal with overlaid the 20 K PL emission of $Eu^{3+}$ in the same material upon the 395 nm excitation (blue line). The a, b, c, d, e depict the zero-phonon excitation lines related to the Stark levels of the $^7F_{0\text{-}6}$ core configuration of the $4f^6(^7F_{0\text{-}6})5d^1$ excited state. Assignment of ZPLs marked with question marks are uncertain. (For interpretation of the references to color in this figure legend, the reader is referred to the Web version of this article.)

summarized in Table S1 which presents the positions of the zero-phonon lines and corresponding vibronic lines assigned to the $^8S_{7/2} \rightarrow 4f^6(^7F_J)5d^1$ transitions.

It is noteworthy that the position of the corresponding zero-phonon lines in the emission and excitation spectra at 20 K are always at slightly shorter wavelengths (higher energy) in $YPO_4$:Eu,Hf than those in $LuPO_4$:Eu,Hf. As discussed above for the ZPL in the emission spectrum, this can be explained by slightly larger crystal field in $LuPO_4$ induced by the shorter Lu–O distances in $LuPO_4$ (2.262(10) and 2.344(10) Å) compared to the Y–O distances in $YPO_4$ (2.300(3) Å and 2.373(3) Å) [34]. This difference is expected to shift the lowest (emitting) 5d level of the $4f^6(^7F_J)5d^1$ excited state to lower energies resulting in a lower energy position of all $4f^6(^7F_J)5d^1$ lines for the lowest energy 5d state.

In both the emission and excitation spectra at 20 K the zero-phonon line is the strongest and, thus, the Stokes shift of the emission would be 0 $cm^{-1}$ (excitation and emission maxima coincide). The Stokes shift can also be estimated from the relative intensity of the vibronic lines giving a value for the Huang-Rhys parameter, $S$ [41,43,51,52]. Following this method for $LuPO_4$:Eu,Hf, a Huang-Rhys parameter $S = 1.86$ was found, which is larger than what we reported for X-ray irradiated $LuPO_4$:$Eu^{2+}$ where $S = 1.42$ [27]. This could be caused by some re-absorption of the ZPL emission in the single crystal used here which lowers the relative ZPL intensity. As the positions of the ZPLs and vibronic lines in $LuPO_4$:Eu,Hf and the irradiated ceramic $LuPO_4$:Eu are exactly the same, the $Eu^{2+}$ canters are equivalent and this indicates that the charge compensation of $Eu^{2+}$ by $Hf^{4+}$ is distant and no locally charge compensated $Eu^{2+}$-$Hf^{4+}$ centers are formed. For this situation, the Huang-Rhys parameters are expected to be the same for the two $LuPO_4$:$Eu^{2+}$ samples.

In the case of $YPO_4$:Eu,Hf single crystal, the relative intensity of the vibronic lines is slightly lower and corresponds to a Huang-Rhys parameter $S = 1.33$. Based on the relative intensities, the Huang-Rhys factor for the $Eu^{2+}$ centers in the orthophosphates is ~1.4 and, with an average phonon energy of ~500 $cm^{-1}$, this corresponds to a Stokes shift of ~1000 $cm^{-1}$ (depending on whether the Stokes is defined as $(2S\text{-}1)\hbar\omega$ or $2S\cdot\hbar\omega$) [41,43,52]. For these small Huang-Rhys parameters, in the weak-coupling regime, it is difficult to define and calculate the Stokes shift. The narrow bandwidth of the emission band at 250 K of ~1000 $cm^{-1}$ is consistent with the estimated small Stokes shift and Huang-Rhys parameter.

For a small Stokes shift, thermal quenching is expected at high temperatures if the quenching mechanism is thermally activated cross-over to the ground in the configurational coordinate diagram. The previously reported thermal quenching for $LuPO_4$:$Eu^{2+}$ indicates that another quenching mechanism is actual [27]. Indeed, usually when $Eu^{2+}$ replaces a trivalent ion, its excited $4f^65d^1$state is seldom located below the bottom of the host conduction band, which is a necessary condition to preclude photo-ionization. In $LuPO_4$ and $YPO_4$, not only the $Eu^{2+}$ is stabilized in the host, but its lowest $4f^65d$ excited state is situated below the conduction band and this makes the observation of $4f^65d \rightarrow 4f^7$ luminescence possible up to about 300 K before being completely quenched via thermally activated photoionization from the $4f^65d$ state to the conduction band [27]. Below, a detailed analysis of the thermal quenching of the $Eu^{2+}$ $4f^65d \rightarrow 4f^7$ luminescence in both $LuPO_4$:Eu,Hf and $YPO_4$:Eu,Hf is presented.

In Fig. 5a and b, the decay curves of the $Eu^{2+}$ emission in $LuPO_4$:Eu,Hf and $YPO_4$:Eu,Hf in the temperature range of 20–300 K are presented. In both materials, the decay traces are almost single-exponential below 200 K. Nevertheless, for a good fit, two decay components are required to correctly reproduce the experimental curves.

The average decay times, <τ>, calculated using Eq. (3) [53–55], are plotted as a function of temperature in Fig. 6.

$$<\tau> = \frac{\int_0^\infty tI(t)\mathrm{d}t}{\int_0^\infty I(t)\mathrm{d}t} = \frac{B_1\tau_1^2 + B_2\tau_2^2}{B_1\tau_1 + B_2\tau_2}, \quad [3]$$

where $B_1$, $B_2$ and $\tau_1$, $\tau_2$ are the pre-exponential factors and decay times, respectively, as determined by fitting the measured decay curves shown in Fig. 5. Below ~200 K, the average decay time is constant and $\tau$ ~210 ns in $LuPO_4$:$Eu^{2+}$,$Hf^{4+}$ and $\tau$ ~225 ns in $YPO_4$:$Eu^{2+}$,$Hf^{4+}$. The slightly longer decay of $Eu^{2+}$ in $YPO_4$ may be assigned to its lower refractive index $n$ ~1.72 [56], compared to that of $LuPO_4$ (ñ1.8–2.0 [57]), which directly affects the decay time according to the Eq. (4) [58–61]:

$$\tau \sim \frac{1}{f(ED)} \frac{\lambda_0^2}{\left[\frac{1}{3}\left(n^2+2\right)\right]^2 n}, \quad [4]$$

where *f(ED)* is the oscillator strength of the electric dipole transition and λ indicates the wavelength of the emitted light. For the same oscillator strength, a faster decay is expected in a host with a higher refractive index. The decay times are shorter than those commonly observed for $Eu^{2+}$ emission around 430 nm which are ~700–1000 ns [62]. The constant value of the decay time below 200 K suggests that this is the radiative decay time. It is not clear

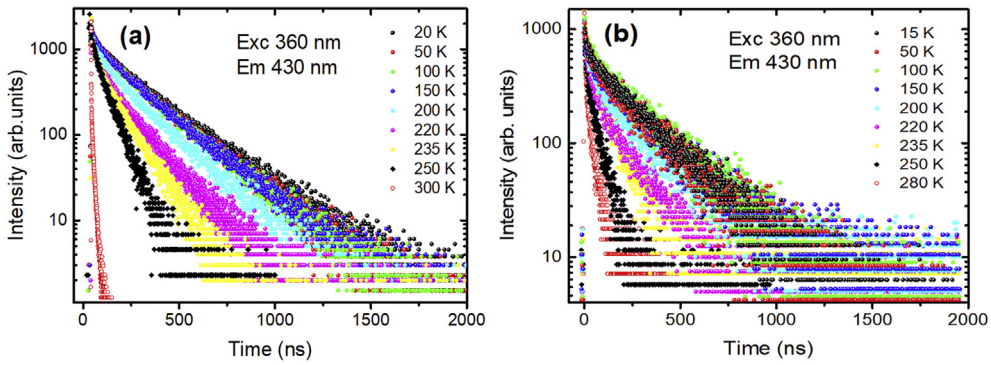


**Fig. 5.** Decay curves of $Eu^{2+}$ emission of $LuPO_4$:Eu,Hf (a) and $YPO_4$:Eu,Hf (b) in the 20–300 K temperature range. Excitation and emission wavelengths are indicated in the Figures.

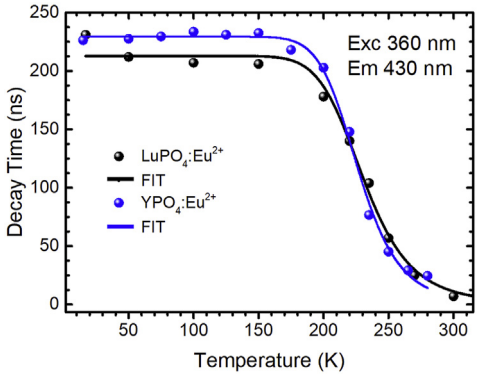


**Fig. 6.** The temperature dependence of the $Eu^{2+}$ decay times (points) of $LuPO_4$:Eu,Hf (black line) and $YPO_4$:Eu,Hf (blue) with a single barrier model fit (lines). (For interpretation of the references to color in this figure legend, the reader is referred to the Web version of this article.)

why the radiative decay time is so much shorter than the commonly observed decay times.

Above 200 K, a continuous shortening of decay times occurs for both crystals and, just above 300 K, the emissions practically disappeared. In Fig. 6, the temperature dependence of the average decay times are presented for the $Eu^{2+}$ emission in both crystals together with the fitting curves obtained with use of Eq. (5) [63,64]:

$$p = \frac{1}{\tau} = \frac{1}{\tau_r} + \frac{1}{\tau_{nr}} exp(-E_a / kT), \quad [5]$$

where $p$ is the transition rate, $\tau$ is its decay time at temperature $T$, $1/\tau_r$ is the probability of radiative transition in the absence of thermal quenching, $1/\tau_{nr}$ is the probability of non-radiative decay, k is the Boltzmann constant and $\Delta E_a$ is the activation energy of thermal quenching. For $LuPO_4$:Eu,Hf, the fitting gives $\Delta E_a = 0.25 \pm 0.01$ eV, while, for $YPO_4$:Eu,Hf, a value of $\Delta E_a = 0.28 \pm 0.02$ eV was obtained. The value determined for the $LuPO_4$:Eu,Hf single crystal is identical to that found in the X-ray irradiated $LuPO_4$:Eu [27]. These energies are in very good agreement with predictions made by Dorenbos of 0.3–0.4 eV (see above) using his model of Vacuum Referred Binding Energies (VRBE) [25,26]. It is thus clear that the mechanism of the thermal quenching is thermally activated ionization of the excited $Eu^{2+}$ as the temperature increases above ~200 K.

Finally, we wish to comment on the just discussed data proving the presence of $Eu^{2+}$ in the Eu,Hf doubly doped $YPO_4$ and $LuPO_4$ crystals in relation to the recently published results of EPR spectroscopy of the same materials [28]. It may be surprising, at first, that EPR spectra did not evidence any clearly resolved signal related to $Eu^{2+}$ in the $YPO_4$:Eu,Hf and $LuPO_4$:Eu,Hf single crystals. $Eu^{2+}$ could be seen by EPR spectroscopy in these materials only after their irradiation with X-rays. Even then, however, the signal from this center presented quite low intensity. In general, EPR spectroscopy is considered as a sensitive tool allowing to detect paramagnetic centers even at low concentrations. Yet, it was already mentioned in the published paper [28] that the EPR signal of $Eu^{2+}$ in the orthophosphates was not easy for detection because of the forbidden character of the involved transitions of this ion. Additionally, many impurities present in the crystals due to their growth from flux produced their EPR spectra obscuring the low-intensity lines of the $Eu^{2+}$ activator. Thus, in the case of the two Eu,Hf doubly-doped single crystals, the EPR and PL data are not in any contradiction. All one may claim is that the concentration of $Eu^{2+}$ in the doubly doped single crystals is not very high. It might be interesting to find out if the growth of the Eu,Hf doubly doped single crystals in an inert or reducing atmosphere of, for example, nitrogen or nitrogen-hydrogen, could increase the $Eu^{2+}$ concentration.

## 4. Conclusions

In this study, we have shown that Eu ions may be stabilized in their divalent state when doped into $LuPO_4$ and $YPO_4$ single crystalline hosts and remain stable for basically an infinite time. The key factor to accomplish $Eu^{2+}$ substitution into $Lu^{3+}$ or $Y^{3+}$ sites in these orthophosphates is co-doping with $Hf^{4+}$ to provide charge compensation according to the $2\,Lu^{X}_{Lu}/Y^{X}_{Y} = Eu'_{Lu} + Hf^{\bullet}_{Lu}$ scheme. The $Eu^{2+}$ dopant in these hosts shows blue d-f luminescence with a FWHM of only ~20 nm at 250 K. At 20 K, the $4f^6 5d \rightarrow 4f^7$ emission consisted of a set of narrow lines. The highest energy, most intense and narrowest $Eu^{2+}$ emission line is located at 425.80 nm (in $LuPO_4$) and 424.40 nm (in $YPO_4$) and is assigned to the zero-phonon line (ZPL). Weaker narrow lines at longer wavelengths result from vibronic transitions in which different lattice phonons were involved. At 20 K, the excitation spectrum of this emission was composed of a large number of narrow lines split into seven groups. The narrowest lines resulted from the $^8S_{7/2} \rightarrow 4f^6(^7F_J)5d^1$ electronic transitions to different $^7F_J$ (J = 0–6) and revealed the $Eu^{3+}$-like $^7F_J$ splitting in the $4f^6(^7F_J)5d^1$ excited configuration of $Eu^{2+}$. Analysis of the low temperature PLE spectra allowed assignment of all the experimentally observed ZPLs of the $^8S_{7/2} \rightarrow 4f^6(^7F_J)5d^1$ transition to the various $4f^6(^7F_{0\text{-}6})$ core states of the $4f^6(^7F_J)5d^1$ excited configuration.

## CRediT authorship contribution statement

**Justyna Zeler:** Writing - original draft. **Megi Sulollari:** Writing - original draft. **Andries Meijerink:** Conceptualization, Writing -

review & editing. **Marco Bettinelli:** Writing - review & editing. **Eugeniusz Zych:** Methodology, Writing - original draft.

## Declaration of competing interest

The authors declare that they have no known competing financial interests or personal relationships that could have appeared to influence the work reported in this paper.

## Acknowledgements

Erica Viviani (Univ. Verona) is gratefully acknowledged for expert technical assistance in the crystal growth.

## Appendix A. Supplementary data

Supplementary data to this article can be found online at https://doi.org/10.1016/j.jallcom.2020.156096.

## References

[1] P. Leblans, L. Struye, S. Elen, I. Mans, H. Vrielinck, F. Callens, X-ray enhancement of CsI:$Eu^{2+}$ radioluminescence, J. Lumin. 165 (2015) 68–76, https://doi.org/10.1016/j.jlumin.2015.04.016.
[2] X. Meng, Y. Wang, H. Jin, L. Sun, A new promising X-ray storage phosphor BaBrCl:$Eu^{2+}$, J. Rare Earths 24 (2006) 503–505, https://doi.org/10.1016/S1002-0721(06)60151-8.
[3] J. Rubio O, Doubly-valent rare-earth ions in halide crystals, J. Phys. Chem. Solid. 52 (1991) 101–174, https://doi.org/10.1016/0022-3697(91)90062-5.
[4] P. Pust, V. Weiler, C. Hecht, A. Tücks, A.S. Wochnik, A.-K. Henß, D. Wiechert, C. Scheu, P.J. Schmidt, W. Schnick, Narrow-band red-emitting Sr[$LiAl_3N_4$]:$Eu^{2+}$ as a next-generation LED-phosphor material, Nat. Mater. 13 (2014) 891–896, https://doi.org/10.1038/nmat4012.
[5] P. Dorenbos, Energy of the first $4f^7 \rightarrow 4f^6$5d transition of $Eu^{2+}$ in inorganic compounds, J. Lumin. 104 (2003) 239–260, https://doi.org/10.1016/S0022-2313(03)00078-4.
[6] W. Tang, Z. Zhang, Realization of color tuning via solid-solution and energy transfer in $Ca_{3-x}Sr_x(PO_4)_2$ :$Eu^{2+}$ ,$Mn^{2+}$ phosphors, J. Mater. Chem. C. 3 (2015) 5339–5346, https://doi.org/10.1039/C5TC00562K.
[7] S. Tamboli, P.D. Bhoyar, S.J. Dhoble, Analysis of electron-vibrational interaction in the 5d states of $Eu^{2+}$ ions in $A_3P_4O_{13}$ and $A_3(PO_4)_2$ (A=Sr, Ba) phosphors, J. Lumin. 184 (2017) 23–28, https://doi.org/10.1016/j.jlumin.2016.12.003.
[8] Y. Zhu, Y. Liang, S. Liu, X. Wu, R. Xu, K. Li, New insight into the structure evolution and site preferential occupancy of $Na_2Ba_6(Si_2O_7)(SiO_4)$2:$Eu^{2+}$ phosphor by cation substitution effect, J. Alloys Compd. 698 (2017) 49–59, https://doi.org/10.1016/j.jallcom.2016.12.195.
[9] Y. Wei, C.C. Lin, Z. Quan, M.S. Molokeev, V.V. Atuchin, T.-S. Chan, Y. Liang, J. Lin, G. Li, Structural evolution induced preferential occupancy of designated cation sites by $Eu^{2+}$ in $M_5(Si_3O_9)_2$ (M = Sr, Ba, Y, Mn) phosphors, RSC Adv. 6 (2016) 57261–57265, https://doi.org/10.1039/C6RA11681G.
[10] X. Li, Y. Hua, H. Ma, D. Deng, S. Xu, Modification of the crystal structure of $Sr_{2-x}Ba_x$ $Si(O,N)_4$:$Eu^{2+}$ phosphors to improve their luminescence properties, CrystEngComm 17 (2015) 9123–9134, https://doi.org/10.1039/c5ce01605c.
[11] Z. Xia, Y. Zhang, M.S. Molokeev, V.V. Atuchin, Y. Luo, Linear structural evolution induced tunable photoluminescence in clinopyroxene solid-solution phosphors, Sci. Rep. 3 (2013) 3310, https://doi.org/10.1038/srep03310.
[12] G. Li, C.C. Lin, W.-T. Chen, M.S. Molokeev, V.V. Atuchin, C.-Y. Chiang, W. Zhou, C.-W. Wang, W.-H. Li, H.-S. Sheu, T.-S. Chan, C. Ma, R.-S. Liu, Photoluminescence tuning via cation substitution in oxonitridosilicate phosphors: DFT calculations, different site occupations, and luminescence mechanisms, Chem. Mater. 26 (2014) 2991–3001, https://doi.org/10.1021/cm500844v.
[13] H. Ji, Z. Huang, Z. Xia, M.S. Molokeev, V.V. Atuchin, M. Fang, Y. Liu, Discovery of new solid solution phosphors via cation substitution-dependent phase transition in $M_3(PO_4)_2$:$Eu^{2+}$ (M= Ca/Sr/Ba) quasi-binary sets, J. Phys. Chem. C 119 (2015) 2038–2045, https://doi.org/10.1021/jp509743r.
[14] C. Zhao, Z. Xia, S. Yu, Thermally stable luminescence and structure evolution of (K, Rb)$BaPO_4$:$Eu^{2+}$ solid-solution phosphors, J. Mater. Chem. C. 2 (2014) 6032–6039, https://doi.org/10.1039/C4TC00488D.
[15] W. Tang, Y. Zheng, Synthesis and luminescence properties of a novel blue emitting phosphor $NaMgPO_4$:$Eu^{2+}$, Luminescence 25 (2010) 364–366, https://doi.org/10.1002/bio.1158.
[16] Z.C. Wu, J.X. Shi, J. Wang, M.L. Gong, Q. Su, A novel blue-emitting phosphor $LiSrPO_4$:$Eu^{2+}$ for white LEDs, J. Solid State Chem. 179 (2006) 2356–2360, https://doi.org/10.1016/j.jssc.2006.04.030.
[17] Y.-S. Tang, S.-F. Hu, C.C. Lin, N.C. Bagkar, R.-S. Liu, Thermally stable luminescence of $KSrPO_4$:$Eu^{2+}$ phosphor for white light UV light-emitting diodes, Appl. Phys. Lett. 90 (2007) 151108, https://doi.org/10.1063/1.2721846.
[18] S. Zhang, Y. Huang, H.J. Seo, The spectroscopy and structural sites of $Eu^{2+}$ ions doped $KCaPO_4$ phosphor, J. Electrochem. Soc. 157 (2010) J261, https://doi.org/10.1149/1.3429887.
[19] Z. Yang, G. Yang, S. Wang, J. Tian, X. Li, Q. Guo, G. Fu, A novel green-emitting phosphor $NaCaPO_4$:$Eu^{2+}$ for white LEDs, Mater. Lett. 62 (2008) 1884–1886, https://doi.org/10.1016/j.matlet.2007.10.030.
[20] P. Dorenbos, Locating lanthanide impurity levels in the forbidden band of host crystals, J. Lumin. 108 (2004) 301–305, https://doi.org/10.1016/j.jlumin.2004.01.064.
[21] R.D. Shannon, Revised effective ionic radii and systematic studies of interatomic distances in halides and chalcogenides, Acta Crystallogr. A 32 (1976) 751–767, https://doi.org/10.1107/S0567739476001551.
[22] L. Havlák, J. Bárta, M. Buryi, V. Jarý, E. Mihóková, V. Laguta, P. Boháček, M. Nikl, $Eu^{2+}$ stabilization in YAG structure: optical and electron paramagnetic resonance study, J. Phys. Chem. C 120 (2016) 21751–21761, https://doi.org/10.1021/acs.jpcc.6b06397.
[23] H.M.H. Fadlalla, C.C. Tang, E.M. Elssfah, F. Shi, Synthesis and characterization of single crystalline YAG:Eu nano-sized powder by sol-gel method, Mater. Chem. Phys. 109 (2008) 436–439, https://doi.org/10.1016/j.matchemphys.2007.12.012.
[24] Q.Q. Zhu, W.W. Hu, L.C. Ju, L.Y. Hao, X. Xu, S. Agathopoulos, Synthesis of $Y_3Al_5O_{12}$:$Eu^{2+}$ phosphor by a facile hydrogen iodide-AssistedSol-gel method, J. Am. Ceram. Soc. 96 (2013) 701–703, https://doi.org/10.1111/jace.12222.
[25] P. Dorenbos, Modeling the chemical shift of lanthanide 4 f electron binding energies Pieter, Phys. Rev. B 85 (2012) 165107, https://doi.org/10.1103/PhysRevB.85.165107.
[26] P. Dorenbos, Charge transfer bands in optical materials and related defect level location, Opt. Mater. 69 (2017) 8–22, https://doi.org/10.1016/j.optmat.2017.03.061.
[27] J. Zeler, A. Meijerink, D. Kulesza, E. Zych, Fine structure in high resolution $4f^7$–$4f^6$5d excitation and emission spectra of X-ray induced $Eu^{2+}$ centers in $LuPO_4$:Eu sintered ceramics, J. Lumin. 207 (2019) 435–442, https://doi.org/10.1016/j.jlumin.2018.11.050.
[28] V. Laguta, M. Buryi, M. Nikl, J. Zeler, E. Zych, M. Bettinelli, Electron and hole trapping in Eu- or Eu,Hf-doped $LuPO_4$ and $YPO_4$ tracked by EPR and TSL spectroscopy, J. Mater. Chem. C. 7 (2019) 11473–11482, https://doi.org/10.1039/C9TC03507A.
[29] A. Lempicki, E. Berman, A.J. Wojtowicz, M. Balcerzyk, L.A. Boatner, Cerium-doped orthophosphates: new promising scintillators, IEEE Trans. Nucl. Sci. 40 (1993) 384–387, https://doi.org/10.1109/23.256585.
[30] L.A. Boatner, Synthesis, structure, and properties of monazite, pretulite, and xenotime, Rev. Mineral. Geochem. 48 (2002) 87–121, https://doi.org/10.2138/rmg.2002.48.4.
[31] G.M. Williams, P.C. Becker, J.G. Conway, N. Edelstein, L.A. Boatner, M.M. Abraham, Intensities of electronic Raman scattering between crystal-field levels of $Ce^{3+}$ in $LuPO_4$: nonresonant and near-resonant excitation, Phys. Rev. B 40 (1989) 4132–4142, https://doi.org/10.1103/PhysRevB.40.4132.
[32] A. Rapaport, V. David, M. Bass, C. Deka, L. Boatner, Optical spectroscopy of erbium-doped lutetium orthophosphate, J. Lumin. 85 (1999) 155–161, https://doi.org/10.1016/S0022-2313(99)00060-5.
[33] R.S. Feigelson, Synthesis and single-crystal growth of rare-earth orthophosphates, J. Am. Ceram. Soc. 47 (1964) 257–258, https://doi.org/10.1111/j.1151-2916.1964.tb14409.x.
[34] W.O. Milligan, D.F. Mullica, G.W. Beall, L.A. Boatner, Structural investigations of $YPO_4$, $ScPO_4$, and $LuPO_4$, Inorg. Chim. Acta. 60 (1982) 39–43, https://doi.org/10.1016/S0020-1693(00)91148-4.
[35] N.G. Connelly, R.M. Hartshorn, T. Damhus, A.T. Hutton, Nomenclature of Inorganic Chemistry IUPAC RECOMMENDATIONS 2005, Royal Society of Chemistry, 2005.
[36] A.H. Krumpel, A.J.J. Bos, A. Bessière, E. van der Kolk, P. Dorenbos, Controlled electron and hole trapping in $YPO_4$:$Ce^{3+}$,$Ln^{3+}$ and $LuPO_4$:$Ce^{3+}$,$Ln^{3+}$ (Ln=Sm, Dy, Ho, Er, Tm), Phys. Rev. B 80 (2009), https://doi.org/10.1103/PhysRevB.80.085103, 085103.
[37] L.A. Zavala-Sanchez, G.A. Hirata, E. Novitskaya, K. Karandikar, M. Herrera, O.A. Graeve, Distribution of $Eu^{2+}$ and $Eu^{3+}$ ions in hydroxyapatite: a cathodoluminescence and Raman study, ACS Biomater. Sci. Eng. 1 (2015) 1306–1313, https://doi.org/10.1021/acsbiomaterials.5b00378.
[38] A. Dobrowolska, E. Zych, Spectroscopic characterization of $Ca_3Y_2Si_3O_{12}$:$Eu^{2+}$ ,$Eu^{3+}$ powders in VUV-UV–vis region, J. Phys. Chem. C 116 (2012) 25493–25503, https://doi.org/10.1021/jp306764f.
[39] O.A. Graeve, R. Kanakala, A. Madadi, B.C. Williams, K.C. Glass, Luminescence variations in hydroxyapatites doped with $Eu^{2+}$ and $Eu^{3+}$ ions, Biomaterials 31 (2010) 4259–4267, https://doi.org/10.1016/j.biomaterials.2010.02.009.
[40] N. Kunkel, A. Meijerink, H. Kohlmann, Bright yellow and green Eu(ii) luminescence and vibronic fine structures in $LiSrH_3$, $LiBaH_3$ and their corresponding deuterides, Phys. Chem. Chem. Phys. 16 (2014) 4807, https://doi.org/10.1039/c3cp55102d.
[41] G. Blasse, Vibronic transitions in rare earth spectroscopy, Int. Rev. Phys. Chem. 11 (1992) 71–100, https://doi.org/10.1080/01442359209353266.
[42] G. Blasse, The intensity of vibronic transitions in the spectra of the trivalent europium ion, Inorg. Chim. Acta. 167 (1990) 33–37, https://doi.org/10.1016/S0020-1693(00)83935-3.
[43] M. de Jong, L. Seijo, A. Meijerink, F.T. Rabouw, Resolving the ambiguity in the relation between Stokes shift and Huang–Rhys parameter, Phys. Chem. Chem. Phys. 17 (2015) 16959–16969, https://doi.org/10.1039/C5CP02093J.
[44] P. Savchyn, I. Karbovnyk, V. Vistovskyy, A. Voloshinovskii, V. Pankratov,

M. Cestelli Guidi, C. Mirri, O. Myahkota, A. Riabtseva, N. Mitina, A. Zaichenko, A.I. Popov, Vibrational properties of $LaPO_4$ nanoparticles in mid- and far-infrared domain, J. Appl. Phys. 112 (2012) 124309, https://doi.org/10.1063/1.4769891.

[45] K. Binnemans, Interpretation of europium(III) spectra, Coord. Chem. Rev. 295 (2015) 1–45, https://doi.org/10.1016/j.ccr.2015.02.015.

[46] L. van Pieterson, M.F. Reid, A. Meijerink, Reappearance of fine structure as a probe of lifetime broadening mechanisms in the $4f^N$-> $4f^{N-1}5d$ excitation spectra of $Tb^{3+}$, $Er^{3+}$, and $Tm^{3+}$ in $CaF_2$ and $LiYF_4$, Phys. Rev. Lett. 88 (2002), https://doi.org/10.1103/PhysRevLett.88.067405, 067405.

[47] H. Ramanantoanina, F. Cimpoesu, C. Göttel, M. Sahnoun, B. Herden, M. Suta, C. Wickleder, W. Urland, C. Daul, Prospecting lighting applications with ligand field tools and density functional theory: a first-principles account of the $4f^7$ –$4f^6 5d^1$ luminescence of $CsMgBr_3:Eu^{2+}$, Inorg. Chem. 54 (2015) 8319–8326, https://doi.org/10.1021/acs.inorgchem.5b00988.

[48] M. de Jong, A. Meijerink, L. Seijo, Z. Barandiarán, Energy level structure and multiple $4f^{12}5d^1$ emission bands for $Tm^{2+}$ in halide perovskites: theory and experiment, J. Phys. Chem. C 121 (2017) 10095–10101, https://doi.org/10.1021/acs.jpcc.7b01902.

[49] M. de Jong, D. Biner, K.W. Krämer, Z. Barandiarán, L. Seijo, A. Meijerink, New insights in $4f^{12}5d^1$ excited states of $Tm^{2+}$ through excited state excitation spectroscopy, J. Phys. Chem. Lett. 7 (2016) 2730–2734, https://doi.org/10.1021/acs.jpclett.6b00924.

[50] A. Bronova, T. Bredow, R. Glaum, M.J. Riley, W. Urland, BonnMag: computer program for ligand-field analysis of f n systems within the angular overlap model, J. Comput. Chem. 39 (2018) 176–186, https://doi.org/10.1002/jcc.25096.

[51] S. Lizzo, A.H. Velders, A. Meijerink, G.J. Dirksen, G. Blasse, The luminescence of $Eu^{2+}$ in magnesium fluoride crystals, J. Lumin. 65 (1995) 303–311, https://doi.org/10.1016/0022-2313(95)00080-1.

[52] V. Bachmann, C. Ronda, A. Meijerink, Temperature quenching of yellow $Ce^{3+}$ luminescence in YAG:Ce, Chem. Mater. 21 (2009) 2077–2084, https://doi.org/10.1021/cm8030768.

[53] M.N. Berberan-Santos, E.N. Bodunov, B. Valeur, Mathematical functions for the analysis of luminescence decays with underlying distributions 1. Kohlrausch decay function (stretched exponential), Chem. Phys. 315 (2005) 171–182, https://doi.org/10.1016/j.chemphys.2005.04.006.

[54] P. Boutinaud, P. Putaj, R. Mahiou, E. Cavalli, A. Speghini, M. Bettinelli, Quenching of lanthanide emission by intervalence charge transfer in crystals containing closed shell transition metal ions, Spectrosc. Lett. 40 (2007) 209–220, https://doi.org/10.1080/00387010701247019.

[55] A. Dobrowolska, E. Zych, Luminescence of Tb-doped $Ca_3Y_2(Si_3O_9)_2$ oxide upon UV and VUV synchrotron radiation excitation, J. Solid State Chem. 184 (2011) 1707–1714, https://doi.org/10.1016/j.jssc.2011.05.014.

[56] A.K. Parchur, G.S. Okram, R.A. Singh, R. Tewari, L. Pradhan, R.K. Vatsa, R.S. Ningthoujam, D.K. Aswal, A.K. Debnath, Effect of EDTA on luminescence property of $Eu^{3+}$ doped $YPO_4$ nanoparticles, in: AIP Conf. Proc., 2010, pp. 391–393, https://doi.org/10.1063/1.3530556.

[57] J. Nipko, C.-K. Loong, M. Loewenhaupt, W. Reichardt, M. Braden, L. Boatner, Lattice dynamics of $LuPO_4$, J. Alloys Compd. 250 (1997) 573–576, https://doi.org/10.1016/S0925-8388(96)02566-2.

[58] R.S. Meltzer, S.P. Feofilov, B. Tissue, H.B. Yuan, Dependence of fluorescence lifetimes of $Y_2O_3:Eu^{3+}$ nanoparticles on the surrounding medium, Phys. Rev. B 60 (1999) R14012–R14015, https://doi.org/10.1103/PhysRevB.60.R14012.

[59] B. Henderson, G.F. Imbusch, Optical Spectroscopy of Inorganic Solids, Oxford science publications, Clarendon Press, 1989.

[60] A. Lempicki, A.J. Wojtowicz, Fundamental limitations of scintillators, J. Lumin. 60–61 (1994) 942–947, https://doi.org/10.1016/0022-2313(94)90317-4.

[61] A. Bednarkiewicz, M. Mączka, W. Strek, J. Hanuza, M. Karbowiak, Size dependence on infrared spectra of $NaGdF_4$ nanocrystals, Chem. Phys. Lett. 418 (2006) 75–78, https://doi.org/10.1016/j.cplett.2005.11.090.

[62] S.H.M. Poort, A. Meyerink, G. Blasse, Lifetime measurements in $Eu^{2+}$-doped host lattices, J. Phys. Chem. Solid. 58 (1997) 1451–1456, https://doi.org/10.1016/S0022-3697(97)00010-3.

[63] M. Yamaga, Y. Ohsumi, T. Nakayama, T.P.J. Han, Persistent phosphorescence in Ce-doped $Lu_2SiO_5$, Opt. Mater. Express 2 (2012) 413, https://doi.org/10.1364/OME.2.000413.

[64] A.K. Prasad, M. Kook, M. Jain, Probing metastable $Sm^{2+}$ and optically stimulated tunnelling emission in $YPO_4$:Ce, Sm, Radiat. Measure 106 (2017) 61–66, https://doi.org/10.1016/j.radmeas.2016.11.012.